Three-Dimensional Curve Reconstruction Based on Material Frame and Twisted Multicore Fiber

Keyuan Yang, Changjian Ke, *Member, IEEE*, Jinrong Tian, Jinxin Liu, Zhen Guo, and Deming Liu

***Abstract*—We propose a curve reconstruction model based on material frame and twisted multicore fiber (MCF), which can reconstruct the position and orientation of MCF simultaneously. The twisted MCF is approximated as a ribbon, whose centerline and surface characteristics are used to characterize the position and orientation of MCF. Material frame corresponding to the ribbon is established, and quantitative analysis is realized by the differential equations between frame basis vectors and fiber deformation parameters. Bending, twisting-strain model is established according to the approximate development of the twisted MCF, and the deformation parameters are obtained. Further, position and orientation of MCF can be reconstructed under the interference of twisting deformation. In simulation, the influence of curvature, torsion of target curves and twist bias, twisting deformation of MCF on curve reconstruction is analyzed. The results indicate that the proposed model is applicable to curves with zero curvature and variable curvature. With 10 rad/m sinusoidal twisting deformation, the deterioration of reconstruction accuracy can be effectively suppressed by introducing twist bias into MCF. For S-shaped curve with curvature and torsion within 1–50 m^{-1} and −10-10 rad/m, the tip position error and tip orientation error are less than 5 mm and 5 mrad over the length of 1 m.**

***Index Terms*—Curve reconstruction, material frame, twisted multicore fiber, position, orientation, bending deformation, twisting deformation, zero curvature, variable curvature.**

I. Introduction

FLEXIBLE manipulators are commonly used in minimally-invasive surgery (MIS) for their high steerability and capability to increase the operation space within limited anatomical regions [1], [2], [3], [4]. In MIS, the flexible manipulator is inserted into the patient's body via the access port and needs to operate dexterously inside the body cavity. In addition, the external force in the radial direction of the manipulator may cause twisting deformation, which will affect the work of the effector. Therefore, obtaining the position and orientation information of the instrument is the basis for correct manipulation [5]. After implanting MCF into the flexible manipulator, centerline and rotation motion of cross-section are obtained through three-dimensional(3D) curve reconstruction, the position and orientation of MCF can be reconstructed simultaneously, which is a compact and efficient solution.

3D curve reconstruction technology based on MCF mainly includes strain sensing technology, deformation-strain model and curve reconstruction algorithm. In the part of strain sensing technology, distributed sensing technology based on Rayleigh scattering or Brillouin scattering, and quasi-distributed sensing technology based on fiber Bragg grating (FBG) can be used to obtain strain information [7], [8], [9]. The deformation-strain model and curve reconstruction algorithm largely determine the accuracy and applicability of the model. In [10], bending-strain model is established based on MCF with straight cores, and the centerline is reconstructed through Frenet-Serret frame. The position information is obtained, but the orientation of MCF cannot be reconstructed. To avoid the singularities of Frenet-Serret frame at zero-curvature position, parallel transport frame [11] and transformation matrices [12], [13] are proposed to reconstruct the centerline, which can improve the applicability of the algorithm, but still cannot reconstruct the orientation of MCF. In [14], bending, twisting-strain model is established based on MCF with straight cores. Position and orientation of MCF are reconstructed through material frame. However, this method requires the twisting direction of MCF to be known, which has certain limitations. To solve the problem that the MCF with straight cores cannot distinguish the twisting direction, a twisted MCF with helical outer cores is used to establish the bending, twisting-strain model. Decorrelation of bending and twisting deformation is realized with unknown twisting direction [15]. In [16], [17], bending, twisting-strain model is established based on a twisted MCF, which improves the accuracy of 3D curve reconstruction by compensating twisting deformation. Then centerline is reconstructed through Frenet-Serret frame. However, the orientation of MCF still cannot be reconstructed, and Frenet-Serret frame suffers singularities at zero-curvature position. Hence, to the best of our knowledge, current 3D curve reconstruction methods still face challenges in obtaining position and orientation information of MCF, reconstructing curves with zero-curvature position and resisting interference of twisting deformation.

In this paper, we propose a curve reconstruction model based on material frame and twisted MCF. The proposed model

Manuscript received 16 July 2022; revised 5 September 2022; accepted 15 September 2022. Date of publication 19 September 2022; date of current version 10 October 2022. This work was supported by the National Natural Science Foundation of China under Grant 61975063. *(Corresponding author: Changjian Ke.)*

Keyuan Yang, Jinrong Tian, and Jinxin Liu are with the School of Optical and Electronic Information, Huazhong University of Science and Technology, Wuhan 430074, China (e-mail: yangky@hust.edu.cn; tjr1997@hust.edu.cn; m202072291@hust.edu.cn).

Zhen Guo is with the Hunan Greatwall Hiden Optical Fiber Technology Company Limited, Changsha 410205, China (e-mail: guoz_hd2021@163.com).

Changjian Ke and Deming Liu are with the School of Optical and Electronic Information, Huazhong University of Science and Technology, Wuhan 430074, China, and also with the Wuhan National Laboratory for Optoelectronics, Wuhan 430074, China (e-mail: cjke@mail.hust.edu.cn; dmliu@mail.hust.edu.cn).

Digital Object Identifier 10.1109/JPHOT.2022.3207599

approximates the twisted MCF as a ribbon, and the position and orientation of the MCF are characterized by the centerline and surface characteristics of the ribbon, respectively. Material frame is established according to the geometric characteristics of the ribbon, the differential equations between the frame basis vectors and the fiber deformation parameters are obtained. The trajectory and rotation motion of the material frame are used to analyze the centerline and surface characteristics of the ribbon quantitatively. Then, the twisted MCF with bending and twisting deformation is approximately developed. Bending, twisting-strain model is established according to the development and the deformation parameters of the twisted MCF are obtained. Further, by substituting the deformation parameters into the differential equations, the trajectory and rotation motion of the material frame are obtained to reconstruct the position and orientation of MCF. Finally, the proposed model is verified in the simulation.

II. Theory

A. Material Frame for Twisted MCF

To manipulate the flexible manipulator correctly, MCF is implanted into the manipulator, the position and orientation are reconstructed through 3D curve reconstruction. In working process, the flexible manipulator will be bent and twisted simultaneously. Twisting deformation has uncertain magnitude and direction under the interference of external force. MCF with straight cores cannot distinguish the twisting direction, which will introduce large error. Therefore, MCF with helical outer cores is used in this paper, which has different response to twisting deformation with different magnitude and direction. Accurate measurement of twisting deformation is realized, which can improve the accuracy of 3D curve reconstruction. Although the MCF with straight outer cores and helical outer cores have different core distribution, the fibers are slender elastic rods in overall size, whose two dimensions are comparable to each other and much smaller than that along the length. Since the two dimensions in the cross-section are not separated, the rotation motion of the cross-section cannot be characterized. In this paper, one dimension in the cross-section is ignored, and the other dimension of the cross-section and that along the length are retained. MCF is approximated as a ribbon with low ratio of width to length and negligible thickness, which separates all three dimensions from each other. Then the position and orientation are reconstructed utilizing the centerline and surface characteristic of the ribbon.

Fig. 1(a) shows the geometric characteristics of a twisted MCF under different deformations. State 1 is the twisted MCF without deformation, whose outer cores are in right-handed helical distribution. The direction of twist bias is defined as positive. The ribbon corresponding to the undeformed twisted MCF is straight and flat. State 2 is the twisted MCF with pure twisting, and the direction of twisting is negative, i.e., opposite to the twist bias. The pitch of the outer cores increases. The surface of the ribbon rotates around the centerline, and the direction and rate of the rotation are the same as the twisting deformation. However, the centerline of the ribbon is still a straight line. On the contrary, if the twisting direction is positive,

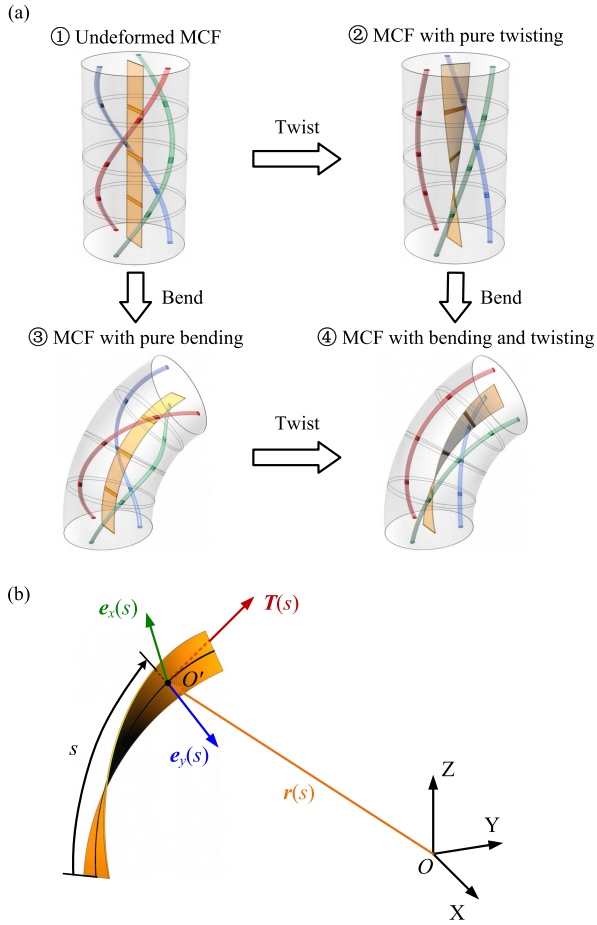

Fig. 1. Schematic diagram of material frame for twisted MCF: (a) Twisted MCF with different deformation and corresponding ribbon; (b) Material frame based on the geometric characteristics of the ribbon.

the pitch of the outer cores decreases, and the surface of the ribbon rotates in a positive direction around the centerline. State 3 is the twisted MCF with pure bending, the outer cores will alternately be stretched or compressed. The centerline of ribbon is an arc, and the angle between the surface of the ribbon and the bending direction of the arc remains constant. State 4 is the twisted MCF with bending and negative twisting. Bending and twisting deformation are independent of each other and have an effect on the MCF. With the influence of bending deformation, the outer cores will alternately be stretched or compressed. Due to the negative twisting deformation, the pitch of outer cores will increase. The centerline of the ribbon is an arc and the angle between the surface of the ribbon and bending direction of the arc is constantly changing. Therefore, the centerline and surface characteristics of the ribbon can be used to characterize the position and orientation of the MCF.

To analysis the geometric characteristics of the ribbon quantitatively, a moving frame is established along the length of ribbon. In common methods, Frenet-Serret frame is corresponding to the curvature and torsion of the centerline, which suffers singularity at zero curvature position. Moreover, Frenet-Serret frame does not evolve naturally with the ribbon's physical rotation within the cross section, i.e., the surface characteristics of the ribbon cannot be characterized. To avoid the singularities at zero-curvature

position, parallel transport frame is used to reconstruct the centerline. However, parallel transport frame is still corresponding to the centerline of the ribbon and cannot characterize the surface characteristics. In this paper, material frame is established according to the centerline and surface characteristics of the ribbon, which will evolve naturally with the translation and rotation motion of the ribbon. Therefore, the centerline and surface characteristics of the ribbon can be characterized by the trajectory and rotation motion of the material frame. Then, the position and orientation can be reconstructed simultaneously.

The material frame corresponding to the ribbon is shown in Fig. 1(b). s is the arc length of centerline, $\boldsymbol{r}(s)$ is the coordinate of the centerline in global coordinate system XYZ. $\boldsymbol{T}(s), \boldsymbol{e}_x(s), \boldsymbol{e}_y(s)$ are the basis vectors of the material frame. $\boldsymbol{T}(s)$ is the tangent vector of centerline. The unit vector $\boldsymbol{e}_x(s)$ lies on the surface of the ribbon and will rotate with twisting deformation. The unit vector $\boldsymbol{e}_y(s)$ is perpendicular to $\boldsymbol{T}(s)$ and $\boldsymbol{e}_x(s)$. $\{\boldsymbol{T}(s), \boldsymbol{e}_x(s), \boldsymbol{e}_y(s)\}$ satisfy the right-hand rule. When the fiber undergoes small strains or uniform deformations, the basis vectors $\boldsymbol{T}(s)$, $\boldsymbol{e}_x(s)$ and $\boldsymbol{e}_y(s)$ remain approximately orthonormal, i.e., $\{\boldsymbol{T}(s), \boldsymbol{e}_x(s), \boldsymbol{e}_y(s)\}$ deforms in a rigid manner. The material frame satisfies the following differential equations [18]:

$$\frac{d}{ds}\begin{pmatrix} \boldsymbol{T}(s) \\ \boldsymbol{e}_x(s) \\ \boldsymbol{e}_y(s) \end{pmatrix} = \begin{pmatrix} 0 & \kappa_x(s) & \kappa_y(s) \\ -\kappa_x(s) & 0 & \omega(s) \\ -\kappa_y(s) & -\omega(s) & 0 \end{pmatrix} \begin{pmatrix} \boldsymbol{T}(s) \\ \boldsymbol{e}_x(s) \\ \boldsymbol{e}_y(s) \end{pmatrix} \tag{1}$$

$\omega(s)$ is the speed at which the frame rotates around $\boldsymbol{T}(s)$, corresponding to the rotation rate of the ribbon. $\kappa_x(s)$, $\kappa_y(s)$ are the speed at which the frame rotates around $\boldsymbol{e}_x(s)$ and $\boldsymbol{e}_y(s)$, respectively, corresponding to the component of bending curvature decomposed along $\boldsymbol{e}_x(s)$ and $\boldsymbol{e}_y(s)$.

$$\begin{cases} \kappa_x(s) = \boldsymbol{T}'(s) \cdot \boldsymbol{e}_x(s) = \kappa \cos\alpha(s) \\ \kappa_y(s) = \boldsymbol{T}'(s) \cdot \boldsymbol{e}_y(s) = \kappa \sin\alpha(s) \end{cases} \tag{2}$$

Using the differential equations in (1), the basis vectors of the material frame can be obtained on the premise of obtaining the deformation parameters of the MCF. In addition, the equations in (1) contain 1 order differential of the tangent vector $\boldsymbol{T}(s)$, so the centerline is required to be 2-times continuously differentiable, which is applicable to curves with zero-curvature position. However, the material frame is corresponding to the centerline and surface characteristics simultaneously. In the numerical solution, the translational and rotational degrees of freedom are coupled with each other, which will deteriorate the solution accuracy. Therefore, in this paper, reduced coordinate formulation with a minimum number of degrees of freedom (i.e., parallel transport frame) is used to calculate the centerline. Then the material frame is obtained by its angular deviation from the parallel transport frame [19].

B. Bending, Twisting–Strain Model Based on Twisted MCF

In Section A, the premise of solving the differential equations refer to (1) is obtaining the deformation parameters $\kappa_x(s)$, $\kappa_y(s)$ and $\omega(s)$. Therefore, it is necessary to calculate the fiber deformation parameters according to the measured strain of each core and structure parameters of the MCF, i.e., to establish mathematic model between bending, twisting and strain. Since the MCF with straight cores cannot distinguish the direction of twisting deformation, the twisted MCF with helical outer cores is utilized in this paper. Fig. 2 shows the geometric characteristics of a twisted MCF with bending and twisting deformation. An infinitesimal element with length of ds is selected for analysis. Firstly, according to the definition of material frame $\{\boldsymbol{T}(s), \boldsymbol{e}_x(s), \boldsymbol{e}_y(s)\}$, a unit vector $\boldsymbol{e}_x$ in the cross-section of the MCF is selected as the basis vector. The starting point of $\boldsymbol{e}_x$ is at the center point of cross-section, and $\boldsymbol{e}_x$ will rotate with the cross-section to characterize the rotation motion of the MCF. Then, the local coordinate system $\boldsymbol{e}_x\boldsymbol{e}_y$ is established according to the right-hand rule, as shown in Fig. 2(a). Since the length of the infinitesimal element is extremely short, the bending and twisting deformation are considered unchanged in this region. Λ is the core spacing.

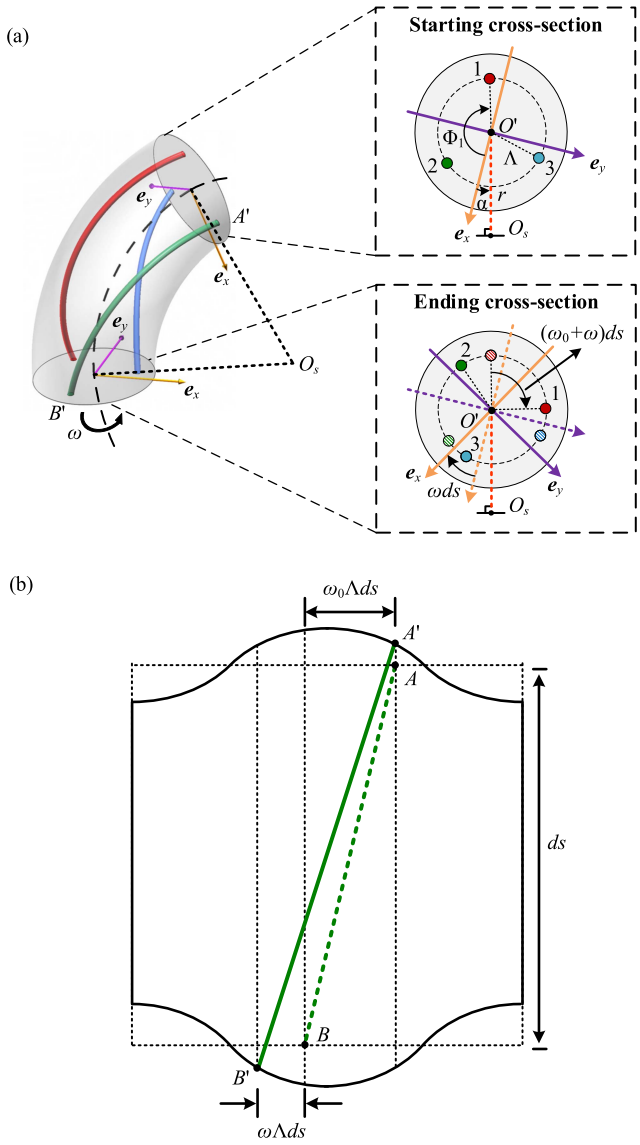

Fig. 2. Schematic diagram of geometric characteristics of a twisted MCF with bending and twisting deformation: (a) 3D stereogram and cross-section diagrams of the infinitesimal element; (b) Development of the infinitesimal element.

α is the angle between the bending direction of MCF and $\boldsymbol{e}_x$. Φ_m is the angle between the *m*-th outer core and $\boldsymbol{e}_x$. ω_0 is the twist bias of the twisted MCF. *O*' is the center of cross-section. O_s is the bending center of the infinitesimal element. *r* is the bending radius. Due to the existence of twisting deformation ω, the ending cross-section of the infinitesimal element rotates at an angle of ωds.

When the twisted MCF is bent and twisted simultaneously, the outer cores rotate around the bent cylinder at a non-uniform speed, which is difficult to analyze. Therefore, the MCF is developed from the inside of the curvature according to the approximate development of undevelopable surface [20]. Fig. 2(b) shows the development of the twisted MCF. Bending deformation of the MCF induces compression on the inside of the curvature and stretch on the outside. The green dotted line $|AB|$ represents the outer core trajectory when the twisted MCF is not deformed, and the green solid line $|A'B'|$ represents the outer core trajectory when the MCF is deformed. According to the geometric relationship in Fig. 2(b), the length of the outer cores before and after deformation can be expressed as:

$$|AB| = ds\sqrt{1+\left(\omega_0\Lambda\right)^2} \tag{3}$$

$$|A'B'| = ds\sqrt{\left[1-\Lambda\kappa\cos\left(\Phi_m-\alpha\right)\right]^2+\left[\left(\omega_0+\omega\right)\Lambda\right]^2} \tag{4}$$

Further according to the definition of strain, the strain of outer cores $\varepsilon_m(s)$ can be obtained:

$$\varepsilon_m(s) = \sqrt{\frac{\left\{1-\Lambda\kappa(s)\cos[\Phi_m(s)-\alpha(s)]\right\}^2+\Lambda^2[\omega_0+\omega(s)]^2}{1+\left(\Lambda\omega_0\right)^2}}-1 \tag{5}$$

$\kappa(s)$ is the curvature of the centerline, $\kappa = 1/r$. *m* represents the *m*-th outer core. According to the geometric relationship in Fig. 2(a) and 2(b), $\Phi_m(0)$ and $\alpha(0)$ are the outer core azimuth and bending direction at the beginning of MCF. Under the influence of twist bias ω_0, twisting deformation ω and torsion τ, $\Phi_m(s)$ and $\alpha(s)$ can be expressed as:

$$\begin{cases}\Phi_m(s) = \Phi_m(0)+\omega_0 s\\ \alpha(s) = \alpha(0)+\int\left[\tau(s)-\omega(s)\right]ds\end{cases} \tag{6}$$

The strain of outer cores with different deformation parameters and structural parameters is calculated by (5) and (6). Both twisting deformation ω and torsion τ change bending direction α, which will affect the strain distribution of each core. If the twisting deformation were not solved accurately, which will introduce large error to the solution of torsion, and then deteriorate the curve reconstruction accuracy. However, solving the bending and twisting parameters by (5) is complicated and prone to multiple solutions. So further approximation and simplification are required.

MCF is a slender rod, whose core spacing is generally within 100 μm. In the application of flexible manipulator and continuous robots, the degree of bending is limited, the curvature of MCF is generally within 100 m^{-1}. Therefore, under the above premise, $|\omega_0+\omega| \ll 1/\Lambda$-$\kappa$, Taylor expansion is applied to (5), and the following approximate results are obtained:

$$\begin{aligned}\varepsilon_m(s) \approx\ & -\Lambda\kappa(s)\cos\left[\Phi_m(s)-\alpha(s)\right]\\ & +\frac{\Lambda^2}{2\sqrt{1+\Lambda^2\omega_0^2}}\left[\omega(s)^2+2\omega_0\omega(s)\right]\end{aligned} \tag{7}$$

The first term on the right side of (7) is the strain component caused by bending and twisting deformation. The second term is the strain component caused by twisting deformation.

The outer cores of MCF are usually symmetrically distributed, i.e., $\Phi_m = \Phi_1 + (m-1)\theta$. $\theta = 2\pi/M$ is the angle between two adjacent outer cores. *M* is the number of outer cores of MCF. $\Phi_1(s)$ is the azimuth of 1st outer core distributed along fiber length. The sum of outer cores strain $\varepsilon_{sum}(s)$ satisfies the following relationship:

$$\begin{aligned}\varepsilon_{sum}(s) &= \frac{M\Lambda^2}{2\sqrt{1+\Lambda^2\omega_0^2}}\left[\omega(s)^2+2\omega_0\omega(s)\right]\\ &\quad+\Lambda\kappa(s)\sin\left[ang(s)\right]\frac{2\cos(\theta/2)\sin(M\theta/2)}{\sin\theta}\\ &= \frac{M\Lambda^2}{2\sqrt{1+\Lambda^2\omega_0^2}}\left[\omega(s)^2+2\omega_0\omega(s)\right]\end{aligned} \tag{8}$$

In (8), $ang(s) = \Phi_1(s)$-$\alpha(s) + (M+1)\theta/2$. $\varepsilon_{sum}(s)$ and $\omega(s)$ satisfy quadratic function relationship, and the axis of symmetry is $\omega = -\omega_0$. When $\omega_0 = 0$, the quadratic function is an even function, resulting in two solutions with equal magnitude and opposite direction, i.e., MCF with straight cores cannot distinguish the direction of twisting deformation. If the twisting deformation with indistinguishable direction is substituted into (1), there will be errors in the solution of the frame basis vectors, which will eventually lead to a large curve reconstruction error. Therefore, $\omega_0 \neq 0$ is required to translate the quadratic function. When the twisting deformation ω is in the monotonic interval of the function, i.e., $-\omega_0 < \omega < \omega_0$, the unique solution of ω can be obtained. $\omega_0 \neq 0$ corresponds to a twisted MCF with helical outer cores, the typical value of twist bias is 50-60turn/m, i.e., 100π–120π rad/m. The typical value of twisting deformation is $-$10-10 rad/m, which meets the above monotonic interval conditions. The solution of twisting deformation can be expressed as:

$$\omega(s) = \sqrt{\omega_0^2+\frac{2\varepsilon_{sum}(s)\sqrt{1+\Lambda^2\omega_0^2}}{M\Lambda^2}}-\omega_0 \tag{9}$$

After computing twisting deformation by (9), the following relationship can be obtained by combining (2) and (7):

$$\begin{aligned}\varepsilon_m(s) =\ & -\Lambda\left[\kappa_x(s)\cos\Phi_m(s)+\kappa_y(s)\sin\Phi_m(s)\right]\\ & +\frac{\Lambda^2}{2\sqrt{1+\Lambda^2\omega_0^2}}\left[\omega(s)^2+2\omega_0\omega(s)\right]\end{aligned} \tag{10}$$

By further transforming (10) with trigonometric function, the expressions of κ_x and κ_y can be obtained:

$$\begin{cases} \kappa_x(s) = -\frac{2}{\Lambda}\sum_{m=1}^{M}\left[\varepsilon_m(s) - \frac{\varepsilon_{sum}(s)}{M}\right]\cos\left[\Phi_m(0) + \omega_0 s\right] \\ \kappa_y(s) = -\frac{2}{\Lambda}\sum_{m=1}^{M}\left[\varepsilon_m(s) - \frac{\varepsilon_{sum}(s)}{M}\right]\sin\left[\Phi_m(0) + \omega_0 s\right] \end{cases} \tag{11}$$

The bending, twisting-strain model is established through (9) and (11), which realizes the solution of deformation parameters. The interference of twisting deformation ω on torsion τ is avoided, and the robustness of curve reconstruction against twisting deformation is effectively improved.

C. Position and Orientation Reconstruction Based on Material Frame and Twisted MCF

After measuring strain of each core by strain sensing technology, the deformation parameters $\kappa_x(s)$, $\kappa_y(s)$ and $\omega(s)$ are obtained by substituting measured strain $\varepsilon_m(s)$ and structural parameters of MCF such as core spacing Λ, azimuth Φ_m, twist bias ω_0 into (9) and (11). Then, the material frame basis vectors $\boldsymbol{T}(s), \boldsymbol{e}_x(s), \boldsymbol{e}_y(s)$ can be obtained by solving the differential equations refer to (1). The centerline of MCF $\boldsymbol{r}$(s) is reconstructed by curve integrating on tangent vector $\boldsymbol{T}(s)$ refer to (12), and the rotation motion of fiber cross-section is described using the direction of unit vector $\boldsymbol{e}_x(s)$, which reconstructs the position and orientation simultaneously.

$$\boldsymbol{r}(s) = \int_0^s \boldsymbol{T}(s)ds + \boldsymbol{r}(0) \tag{12}$$

The complete model proposed in this paper considers the influence of twisting deformation ω on 3D curve reconstruction, and uses a twisted MCF with twist bias ω_0 to obtain the magnitude and direction of twisting deformation simultaneously, which suppresses the deterioration of the accuracy of curve reconstruction effectively. Further, material frame is used to reconstruct the position and orientation of the MCF simultaneously, which is applicable to curves with zero-curvature position and variable curvature. The proposed model can be approximated to reported models in certain conditions. When considering the influence of twisting deformation, i.e., $\omega \neq 0$, using a twisted MCF, i.e., $\omega_0 \neq 0$, and utilizing Frenet-Serret frame for curve reconstruction, the proposed model can be approximated as I. Floris' model. This model can avoid the interference of twisting deformation on curve reconstruction, but cannot describe the rotation motion of cross section and is not applicable to curves with zero-curvature position [16]. When considering the influence of twisting deformation, i.e., $\omega \neq 0$, using an MCF with straight cores, i.e., $\omega_0 = 0$, and utilizing material frame for curve reconstruction, the proposed model can be approximated as V. Modes' model. This model can reconstruct the position and orientation of the MCF and is applicable to curves with zero-curvature position, but has the limitation that the twisting direction must be known in advance [14]. When not considering the influence of twisting deformation, i.e., $\omega = 0$, using an MCF with straight cores, i.e., $\omega_0 = 0$, and utilizing parallel transport frame for curve reconstruction, the proposed model can be approximated as J. Cui's model. This model is applicable to curves with zero-curvature position, but cannot describe the rotation motion of cross section. And twisting deformation will significantly deteriorate the accuracy of curve reconstruction [11]. When the target curve is cubic continuous differentiable, J. Cui's model can be further transformed into J.P. Moore's model, which is not applicable to curves with zero-curvature position [21].

III. Simulation

The complete model for 3D curve reconstruction proposed in this paper is verified in the simulation. Firstly, the strain distribution of each core with different target curves is obtained by (5). Then, the bending and twisting deformation parameters are calculated by (9) and (11). Finally, the centerline and rotation motion of cross section are obtained simultaneously by (1) and (12). In MIS, the curvature and torsion of flexible manipulators are usually not constant, but depend on the position and orientation of the manipulator. Therefore, two typical curves are selected in the simulation. S-shaped curve with zero-curvature position corresponds to the sudden change of bending direction in the work of the manipulator. Conical helix with variable curvature and torsion corresponds to the dynamic curvature and torsion of the manipulator [22], [23]. Three-core MCF with symmetrical core distribution is used in simulation, whose core spacing is 40 μm. Due to the physical properties of optical fiber, the distribution of twisting deformation along the length is random and gradual. Therefore, twisting deformation with sinusoidal distribution along the length is selected in the simulation [24]. Spatial resolution of strain sensing technology is 1 mm. Tip position error and tip orientation error are used to evaluate the performance of curve reconstruction [23]. Performance of different models will be compared in the simulation. Models 1-4 are curve reconstruction models reported in [10], [11], [14], [16], respectively. Model 5 is the model proposed in this paper.

Figs. 3 and 4 shows the reconstruction results of different models for S-shaped curve and conical helix, respectively. Twist bias of the MCF with straight cores and helical cores are 0 and 50 turn/m. The twisting deformation of the MCF is sinusoidal distribution with amplitude of 10 rad/m. The error introduced by curve reconstruction models is mainly analyzed in this section. And the strain measurement error is not considered, which takes a value of 0 $\mu\varepsilon$. The black dash line represents the theoretical curve, and the black dashed arrow represents the theoretical rotation motion of the cross-section. Blue dash dot line, green dash dot dot line, orange dot line, purple short dash dot and red solid line represent the centerlines reconstructed by model 1-5, respectively. The orange dot arrow and red solid arrow represent the rotation motion of cross-section reconstructed by model 3 and model 5, respectively.

In Fig. 3, S-shaped curve with a total length of 1.0 m is obtained by splicing two arcs with same curvature and opposite torsion. The curvature of the arc is 5 m^{-1}, and the torsion is 3 rad/m and -3 rad/m, successively. Fig. 3(a) shows the centerlines and rotation motion of different models for S-shaped curve. The reconstructed centerlines of model 1-4 have large deviation

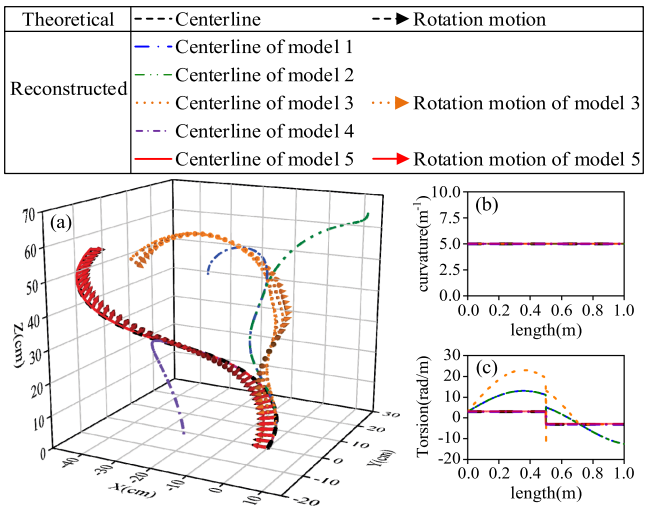

Fig. 3. Reconstruction results of different models for S-shaped curve. The amplitude of sinusoidal twisting deformation is 10 rad/m: (a) Centerlines and rotation motion; (b) Curvature of reconstructed centerlines; (c) Torsion of reconstructed centerlines.

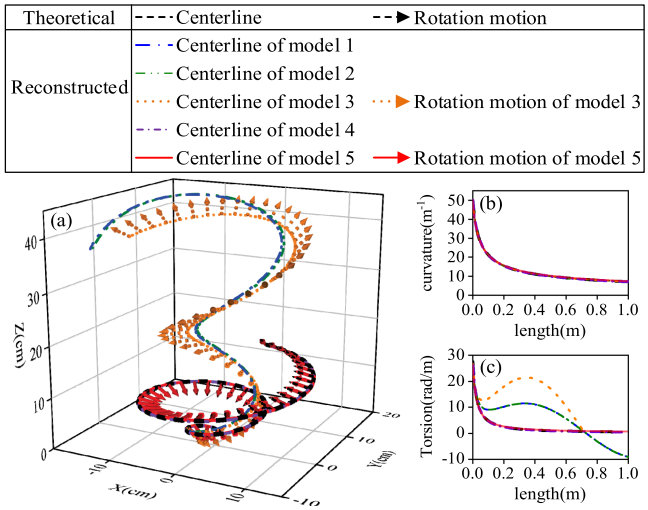

Fig. 4. Reconstruction results of different models for conical helix. The amplitude of sinusoidal twisting deformation is 10 rad/m: (a) Centerlines and rotation motion; (b) Curvature of reconstructed centerlines; (c) Torsion of reconstructed centerlines.

from the theoretical curve. And the centerline reconstructed by model 5 is in good agreement with the theoretical curve. Tip position error of model 1-5 are 787.1 mm, 434.2 mm, 125.0 mm, 267.2 mm and 3.3 mm, respectively. Tip orientation error of model 3 and 5 is 363.8 mrad and 0.24 mrad, respectively. The reason is that model 1-3 use an MCF with straight cores, which can measure the curvature of the twisted MCF correctly, as shown in Fig. 3(b). However, MCF with straight cores cannot distinguish the twisting direction, resulting in large error of torsion, as shown in Fig. 3(c). Eventually, a large tip position error is introduced in model 1-3. Model 4 and 5 use a twisted MCF, which can effectively avoid the interference of twisting deformation on curve reconstruction. However, Frenet-Serret frame is utilized for curve reconstruction in model 4, which suffers singularities at zero-curvature position, so the tip position error is large. Material frame is utilized in model 5, which is applicable to curves with zero-curvature position, resulting in small tip position error. In addition, the rotation motion of cross-section can be obtained by model 3 and model 5. However, MCF with straight cores used in model 3 introduces large error to the rotation motion of cross-section. On the contrary, the rotation motion of cross-section obtained by model 5 is in good agreement with the theoretical value.

In Fig. 4, the curvature of the right-handed conical helix gradually changes from 50.0 m^{-1} to 7.0 m^{-1}, the torsion gradually changes from 27.5 rad/m to 0.5 rad/m, the total length is 1.0 m. Fig. 4(a) shows the centerlines and rotation motion of different models for conical helix. The reconstructed centerlines of model 4 and 5 are in good agreement with the theoretical curve. Tip position error of model 1-5 are 328.7 mm, 326.8 mm, 298.3 mm, 1.5 mm and 2.8 mm, respectively. Tip orientation error of model 3 and model 5 are 363.8 mrad and 0.21 mrad, respectively. The reason is that model 4 and model 5 use a twisted MCF, which can measure the curvature and torsion of the twisted MCF correctly, as shown in Fig. 4(b) and (c). Since there is no zero-curvature position in the conical helix, model 4 using Frenet-Serret frame and model 5 using material frame both can correctly reconstruct the conical helix. The tip position error of conical helix is smaller than that of S-shaped curve, because the sudden change of bending direction in the S-shaped curve introduces additional error. The tip position error of model 4 is smaller than model 5. The main reason is that model 4 uses Frenet-Serret frame for curve reconstruction, whose differential equations have higher solution accuracy. Similarly, the rotation motion of cross-section obtained by model 5 is in good agreement with the theoretical value.

Then, we investigate the influence of curvature and torsion of target curve on the tip position error and tip orientation error, as shown in Fig. 5. For the sake of convenience, S-shaped curve is selected as the target curve. The two arcs that constituting the S-shaped curve have equal curvature and opposite torsion. The curvature and torsion are in the range of 1–50 m^{-1} and −10-10 rad/m, respectively. The length of the curve is still 1 m. Twisting deformation is still sinusoidal distribution along the length with amplitude of 10 rad/m. Twist bias is set to 0, 1, 10, 50turn/m, respectively. When the twist bias is 0turn/m, the direction of twisting deformation cannot be distinguished by (9). The wrong root will lead to errors in curve reconstruction, which increases the tip position error and orientation error, corresponding to the shadow of Fig. 5(a) and 5(b). When the twist bias is 1turn/m, for the twisting deformation with magnitude less than twist bias, its direction can be distinguished by (9). However, for the twisting deformation with magnitude larger than twist bias, there will be wrong roots during solving (9), which will deteriorate the reconstruction accuracy, as shown in Fig. 5(c) and 5(d). Reconstruction accuracy is higher in the region where curvature is small and torsion, twist bias in the same direction. The main reason is that the S-shaped curve with small curvature tends to be a straight segment, and the deterioration of twisting deformation on accuracy is less obvious. At the same time, torsion of the curve will also cause the rotation of the

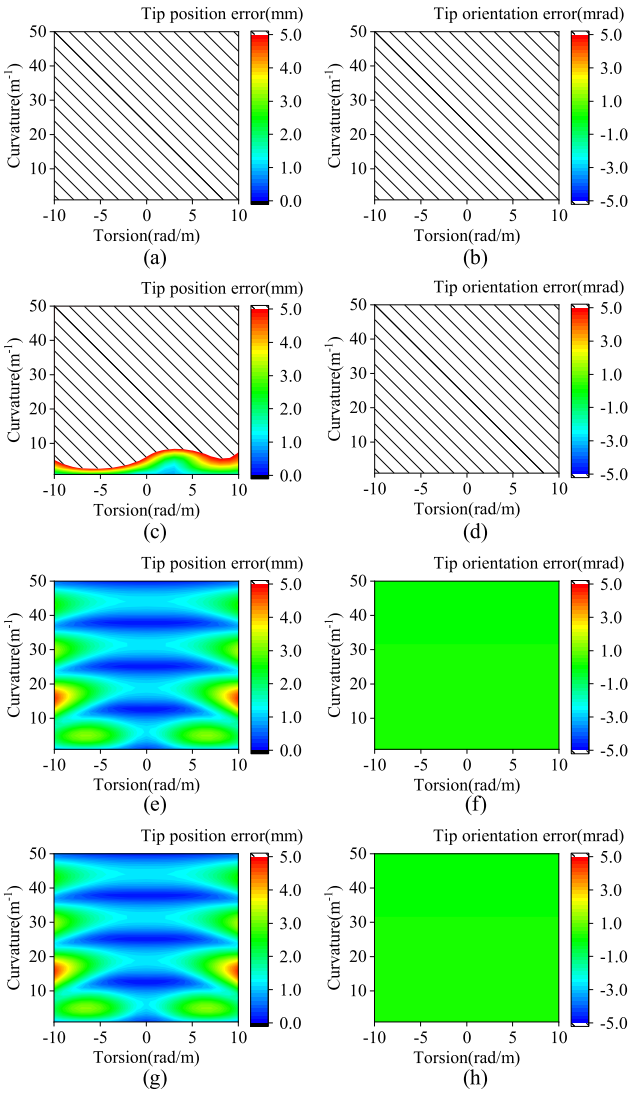

Fig. 5. With different twist bias of MCF, tip position error and tip orientation error of proposed model as a function of curvature and torsion of S-shaped curve. The amplitude of sinusoidal twisting deformation is 10 rad/m: (a), (c), (e), (g) tip position error; (b), (d), (f), (h) tip orientation error; (a), (b) ω_0=0turn/m; (c), (d) ω_0=1turn/m; (e), (f) ω_0=10turn/m; (g), (h) ω_0=50turn/m.

cross section, and torsion with same direction as the twist bias will reduce part of the interference of twisting deformation, thus suppressing the deterioration of reconstruction accuracy. When the twist bias is 10turn/m, the magnitude of twisting deformation is less than the twist bias. Therefore, the magnitude and direction of twisting deformation can be obtained, then the centerline and rotation motion of cross-section can be reconstructed correctly, as shown in Fig. 5(e) and 5(f). In Fig. 5(e), tip position error increases with the increase of magnitude of torsion. The main reason is that torsion of the curve is the derivative of the bending direction. A higher magnitude of torsion means that the bending direction changes faster, which introduces larger error in the curve reconstruction. Tip position error has some periodic fluctuation with the increase of curvature. The main reason is that the arcs constituting the S-shaped curve have spatial periodicity. When the curvature changes, the tip position error will change periodically. In Fig. 5(f), tip orientation error remains basically the same with different twist bias. The main reason is that curvature and torsion correspond to the translational degrees of freedom, tip rotation motion corresponds to the rotational degrees of freedom. Changes of curvature and torsion have little effect on tip orientation error. When the twist bias increases to 50turn/m, the tip position error and tip orientation error in Fig. 5(g) and 5(h) are basically the same as those with twist bias of 10turn/m. On the one hand, the increase of twist bias will increase the demand for the spatial resolution of strain measurement. However, the 1 mm spatial resolution in the simulation can still meet the demand of 50turn/m twist bias, so the curve reconstruction error does not significantly deteriorate. On the other hand, in (8), the increase of twist bias ω_0 will make twisting deformation ω far away from the axis of symmetry. The sensitivity of outer cores strain $\varepsilon_{sum}(s)$ to twisting deformation ω is improved, which can suppress the deterioration of strain measurement error on the curve reconstruction accuracy. Since the strain measurement error is not considered in the simulation, the curve reconstruction error is not significantly optimized. Therefore, the curve reconstruction error with twist bias of 50turn/m is basically consistent with that of 10turn/m. In addition, if the length, curvature and torsion of the two arcs constituting S-shaped curve are different, the error characteristics of the two arcs will be different, and the reconstruction error of the S-shaped curve is the accumulation of that of the two arcs. In general, with twist bias larger than the magnitude of twisting deformation, the proposed model can achieve tip position error less than 5 mm and tip orientation error less than 5 mrad with curvature of 1–50 m^{-1} and torsion of $-$10-10 rad/m.

The model proposed in this paper can reconstruct the centerline and rotation motion of cross-section simultaneously, and is applicable to curves with zero curvature and variable curvature. When the twisting deformation takes a sinusoidal distribution with amplitude of 10 rad/m, the deterioration of curve reconstruction accuracy is effectively suppressed by introducing twist bias into MCF. For S-shaped curve with curvature and torsion in the range of 1–50 m^{-1} and $-$10-10 rad/m, respectively, proposed model can achieve tip position error of less than 5 mm and tip orientation error of less than 5 mrad over the length of 1 m, which could meet the requirements of accuracy in MIS [25], [26]. In addition, by optimizing the numerical method for solving the differential equations corresponding to material frame, reconstruction accuracy of proposed model is expected to be further improved.

IV. Conclusion

In this paper, we propose a curve reconstruction model based on material frame and twisted MCF. The twisted MCF is approximated as a ribbon, whose centerline and surface characteristics are used to characterize the position and orientation of the MCF. Material frame corresponding to the ribbon is established. Differential equations between frame basis vectors and fiber deformation parameters are obtained for quantitative analysis. The twisted MCF with bending and twisting

deformation is approximately developed. Bending, twisting-strain model is established, which obtains the deformation parameters of the twisted MCF. Further, the deformation parameters are substituted into the differential equations to obtain the basis vectors of the material frame. Position and orientation of MCF is reconstructed accurately under the interference of twisting deformation. The simulation results indicate that the proposed model is applicable to S-shaped curve with zero-curvature position and conical helix with variable curvature. When the twisting deformation takes a sinusoidal distribution with amplitude of 10 rad/m, the deterioration of reconstruction accuracy can be suppressed by introducing twist bias into MCF. For S-shaped curve with curvature and torsion in the range of 1–50 m^{-1} and −10-10 rad/m, respectively, the proposed model can achieve tip position error of less than 5 mm and tip orientation error of less than 5 mrad over the length of 1 m. Therefore, the proposed model provides a promising approach for the reconstruction of position and orientation in the working process of flexible manipulators.

REFERENCES

[1] F. Monet et al., "High-resolution optical fiber shape sensing of continuum robots: A comparative study," in *Proc. IEEE Int. Conf. Robot. Automat.*, 2020, pp. 8877–8883.

[2] F. Khan, A. Denasi, D. Barrera, J. Madrigal, S. Sales, and S. Misra, "Multi-core optical fibers with Bragg gratings as shape sensor for flexible medical instruments," *IEEE Sensors J.*, vol. 19, no. 14, pp. 5878–5884, Jul. 2019.

[3] C. Shi et al., "Shape sensing techniques for continuum robots in minimally invasive surgery: A survey," *IEEE Trans. Biomed. Eng.*, vol. 64, no. 8, pp. 1665–1678, Aug. 2017.

[4] L. Wu, S. Song, K. Wu, C. M. Lim, and H. Ren, "Development of a compact continuum tubular robotic system for nasopharyngeal biopsy," *Med. Biol. Eng. Comput.*, vol. 55, no. 3, pp. 403–417, 2017.

[5] D. Ji, T. H. Kang, S. Shim, and J. Hong, "Analysis of twist deformation in wire-driven continuum surgical robot," *Int. J. Control, Automat. Syst.*, vol. 18, no. 1, pp. 10–20, Jan. 2020.

[6] V. Mishra, N. Singh, U. Tiwari, and P. Kapur, "Fiber grating sensors in medicine: Current and emerging applications," *Sensors Actuators A: Phys.*, vol. 167, pp. 279–290, Jun. 2011.

[7] F. Parent et al., "Enhancement of accuracy in shape sensing of surgical needles using optical frequency domain reflectometry in optical fibers," *Biomed. Opt. Exp.*, vol. 8, no. 4, pp. 2210–2221, Apr. 2017.

[8] Z. Guo, C. Xing, C. Ke, K. Yang, and D. Liu, "3D shape sensing utilizing SBS in multi-core fiber," in *Proc. Opt. Fiber Commun. Conf.*, 2019, pp. 1–3.

[9] R. Xu, A. Yurkewich, and R. V. Patel, "Curvature, torsion, and force sensing in continuum robots using helically wrapped FBG sensors," *IEEE Robot. Automat. Lett .*, vol. 1, no. 2, pp. 1052–1059, Jul. 2016.

[10] J. P. Moore and M. D. Rogge, "Shape sensing using multi-core fiber optic cable and parametric curve solutions," *Opt. Exp.*, vol. 20, no. 3, pp. 2967–2973, 2012.

[11] J. Cui, S. Zhao, C. Yang, and J. Tan, "Parallel transport frame for fiber shape sensing," *IEEE Photon. J.*, vol. 10, no. 1, Feb. 2018, Art no. 6801012.

[12] D. Paloschi, K. A. Bronnikov, S. Korganbayev, A. A. Wolf, A. Dostovalov, and P. Saccomandi, "3D shape sensing with multicore optical fibers: Transformation matrices versus frenet-serret equations for real-time application," *IEEE Sensors J.*, vol. 21, no. 4, pp. 4599–4609, Feb. 2021.

[13] R. J. Roesthuis, M. Kemp, J. J. van den Dobbelsteen, and S. Misra, "Three-dimensional needle shape reconstruction using an array of fiber Bragg grating sensors," *IEEE/ASME Trans. Mechatronics*, vol. 19, no. 4, pp. 1115–1126, Aug. 2014.

[14] V. Modes, T. Ortmaier, and J. Burgner-Kahrs, "Shape sensing based on longitudinal strain measurements considering elongation, bending, and twisting," *IEEE Sensors J.*, vol. 21, no. 5, pp. 6712–6723, Mar. 2021.

[15] C. G. Askins, G. A. Miller, and E. J. Friebele, "Bend and twist sensing in a multiple-core optical fiber," in *Proc. Opt. Fiber Commun. Conf./Nat. Fiber Opt. Eng. Conf.*, 2008, pp. 1–3.

[16] I. Floris, J. Madrigal, S. Sales, P. A. Calderón, and J. M. Adam, "Twisting measurement and compensation of optical shape sensor based on spun multicore fiber," *Mech. Syst. Signal Process.*, vol. 140, Jun. 2020, Art. no. 106700.

[17] P. S. Westbrook et al., "Continuous multicore optical fiber grating arrays for distributed sensing applications," *J. Lightw. Technol.*, vol. 35, no. 6, pp. 1248–1252, Mar. 2017.

[18] J. Langer and D. A. Singer, "Lagrangian aspects of the Kirchhoff elastic rod," *SIAM Rev.*, vol. 38, no. 4, pp. 605–618, 1996.

[19] M. Bergou, M. Wardetzky, S. Robinson, B. Audoly, and E. Grinspun, "Discrete elastic rods," *ACM Trans. Graph.*, vol. 27, no. 3, pp. 1–12, 2008.

[20] T. E. French and C. J. Vierck, "Intersections and developments," in *Graphic Science: Engineering Drawing, Descriptive Geometry, Graphical Solutions*. New York, NY, USA: McGraw-Hill, 1963, pp. 552–554.

[21] R. L. Bishop, "There is more than one way to frame a curve," *Amer. Math. Monthly*, vol. 82, no. 3, pp. 246–251, Mar. 1975.

[22] Y. Lu, B. Lu, B. Li, H. Guo, and Y. -H. Liu, "Robust three-dimensional shape sensing for flexible endoscopic surgery using multi-core FBG sensors," *IEEE Robot. Automat. Lett.*, vol. 6, no. 3, pp. 4835–4842, Jul. 2021.

[23] M. Chadha, "Theoretical development of framed space curve and its applications to higher-order geometrically-exact rod theory, shape sensing, path estimation, and computer graphics," Ph.D. dissertation, Dept. Struct. Eng., Univ. California, San Diego, CA, USA, 2019.

[24] M. J. Li and T. Hayashi, "Advances in low-loss, large-area, and multicore fibers," in *Optical Fiber Telecommunications VII*. Cambridge, MA, USA: Academic, 2020, ch. 1, pp. 3–50.

[25] P. Gomes, *Medical Robotics: Minimally Invasive Surgery*. Amsterdam, The Netherlands: Elsevier, 2012.

[26] S. Jäckle et al., "Three-dimensional guidance including shape sensing of a stentgraft system for endovascular aneurysm repair," *Int. J. Comput. Assist. Radiol. Surg.*, vol. 15, no. 6, pp. 1033–1042, May 2020.